Neuron, Vol. 39, 555–568, July 31, 2003, Copyright ©2003 by Cell Press

Stereopsis Activates V3A and Caudal Intraparietal Areas in Macaques and Humans

Doris Y. Tsao,[1,2,*] Wim Vanduffel,[1,4]
Yuka Sasaki,[1,3] Denis Fize,[4]
Tamara A. Knutsen,[1] Joseph B. Mandeville,[1,3]
Lawrence L. Wald,[1] Anders M. Dale,[1,3]
Bruce R. Rosen,[1,3] David C. Van Essen,[5]
Margaret S. Livingstone,[2] Guy A. Orban,[4]
and Roger B.H. Tootell[1,3]
[1]Massachusetts General Hospital
NMR Center
Athinoula A. Martinos Center
Charlestown, Massachusetts 02129
[2]Department of Neurobiology
[3]Department of Radiology
Harvard Medical School
Boston, Massachusetts 02115
[4]Katholieke Universiteit te Leuven
Faculty of Medicine
Laboratorium voor Neuro en Psychofysiologie
B-3000 Leuven
Belgium
[5]Department of Anatomy and Neurobiology
Washington University School of Medicine
St. Louis, Missouri 63110

Summary

Stereopsis, the perception of depth from small differences between the images in the two eyes, provides a rich model for investigating the cortical construction of surfaces and space. Although disparity-tuned cells have been found in a large number of areas in macaque visual cortex, stereoscopic processing in these areas has never been systematically compared using the same stimuli and analysis methods. In order to examine the global architecture of stereoscopic processing in primate visual cortex, we studied fMRI activity in alert, fixating human and macaque subjects. In macaques, we found strongest activation to near/far compared to zero disparity in areas V3, V3A, and CIPS. In humans, we found strongest activation to the same stimuli in areas V3A, V7, the V4d topolog (V4d-topo), and a caudal parietal disparity region (CPDR). Thus, in both primate species a small cluster of areas at the parieto-occipital junction appears to be specialized for stereopsis.

Introduction

Our perception of shapes and surfaces in 3D space is the intuitive basis for our understanding of the physical world. The surface structure of an object provides a powerful identification tool and also indicates how an object should be grasped and handled.

A powerful cue to 3D structure is binocular disparity, the difference between the images in the two eyes. Barlow et al. (1967) and Pettigrew et al. (1968) were the first to study disparity tuning of neurons in the visual cortex, in V1 of the anaesthetized cat. Later, Poggio et al. distinguished five classes of disparity-tuned cells (near, far, zero, tuned excitatory, and tuned inhibitory) in V1, V2, and V3/V3A (Poggio and Fischer, 1977; Poggio et al., 1988) of the alert macaque. Several groups have found that disparity-tuned cells in extrastriate visual areas are organized into "near" and "far" columns (V2, Hubel and Livingstone, 1987; Ts'o et al., 2001; V3, Hubel and Wiesel, 1970; Adams and Zeki, 2001; MT, DeAngelis and Newsome, 1999; V4, Watanabe et al., 2000).

Disparity is a rich cue, sufficient to sculpt any 3D percept imaginable. Disparity specifies not only the depth of each point in the visual array, but also higher-order surface properties such as edges, surface orientation, and shape. Cells sensitive to disparity edges have been reported in areas V2 (Thomas et al., 2002), MT (Bradley and Andersen, 1998), and MSTl (Eifuku and Wurtz, 1999). Tuning to disparity-defined 3D surface orientation and 3D curvature have been found in the caudal intraparietal sulcus (CIPS) (Sakata et al., 1998) and area TEs (Janssen et al., 2000), respectively.

Disparity is also an important cue for driving vergence eye movements (Masson et al., 1997), and several groups have reported disparity-tuned neurons in areas involved in eye-movement coding such as MST (Takemura et al., 2001), LIP (Gnadt and Mays, 1995), and the frontal eye fields (Ferraina et al., 2000).

Typically, single-unit studies have tested sensitivity to a particular higher-order disparity stimulus within a single extrastriate area. Thus, the relative contribution of different areas to coding different higher-order surface properties—the global architecture of stereopsis—remains unclear. Figure 1 shows the percentage of disparity-tuned neurons reported in various extrastriate visual areas. Estimates vary between investigators, and even the same investigator can state differing percentages depending upon the criteria used. Nevertheless, it is fair to say that no one extrastriate area jumps out as "the center" of disparity processing. Rather, the single-unit data suggest that disparity processing is widely distributed throughout the visual cortex.

In contrast to the single-unit data in macaques, several fMRI studies of human visual cortex have found that the BOLD signal elicited during stereopsis is localized to area V3A (Backus et al., 2001; Mendola et al., 1999; Greenlee and Rutschmann, 2000) and cortex adjacent to the intraparietal sulcus (Kwee et al., 1999). Human MT+ was not prominently activated in any of these studies. Some groups have reported additional activation in the lateral occipital complex, in response to random-dot stereograms of complex objects (Gilaie Dotan et al., 2002; Kourtzi and Kanwisher, 2001).

fMRI is perhaps a more appropriate technique for comparative functional neuroanatomy than single-cell recording, since it allows activation to a stimulus to be sampled uniformly across the entire brain of a single subject. In contrast, electrophysiologists over the decades have used different recording methods, stimuli,

*Correspondence: doris@nmr.mgh.harvard.edu

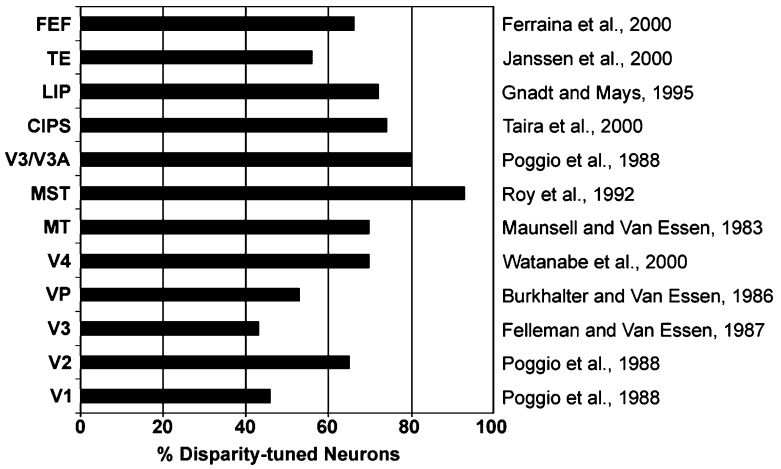

Figure 1. The Percentage of Disparity-Tuned Cells in Different Visual Areas

The areas are listed in roughly hierarchical order, from bottom to top. The percentages are taken from the studies indicated in the right-hand column. For details, see Gonzalez and Perez (1998). The percentage for area TE refers to cells in the lower bank of the STS that are sensitive to disparity-defined 3D shape. The percentage for area CIPS refers to cells that show selectivity for disparity-defined 3D surface orientation. Based on the number of disparity-tuned cells, no single area emerges as an obvious center of disparity processing.

and analysis techniques to study disparity processing within different areas of different animals.

However, the lower resolution of fMRI data, combined with its hemodynamic origin, also opens its meaning to more interpretations. Within each voxel, fMRI samples averaged activity across hundreds of thousands of neurons via hemodynamics. Thus, the net activation of a voxel to a disparity stimulus depends on many factors, including the nature of the disparity-defined variable being encoded, the concentration of disparity-tuned cells, the shape of disparity-tuning curves, the size of functional domains relative to the voxel size, and the precise nature of neural-hemodynamic coupling.

Ultimately, one would like to combine the coarse but comprehensive knowledge about stereoscopic processing derived from fMRI with the confined but precise knowledge derived from single-cell recordings, in order to understand the neural processing of stereopsis in its full breadth and depth. It is difficult to directly compare fMRI studies in humans with electrophysiological studies in macaques, because in such comparisons species differences are confounded with technique differences. Here, for the first time, we examined fMRI activation to stereoscopic stimuli in the visual cortex of the alert macaque monkey and compared it to that in the human.

Results

Activation to Nonzero versus Zero Disparity in Macaques and Humans

Our first experimental goal was to identify areas in macaque and human visual cortex that are more strongly activated by a disparity-rich stimulus compared to uniform zero disparity.

We scanned four macaques and eight humans. The experimental setup for the human and monkey fMRI has been described elsewhere (Tootell et al., 1997; Vanduffel et al., 2001; Leite et al., 2002). In our first experiment, a near/far disparity stimulus alternated with a zero disparity stimulus in a two-condition block design (visual stimuli can be viewed online at http://www.nmr.mgh.harvard.edu/~doris/disparity_fmri.html). The disparity stimulus consisted of a dynamic random-dot stereogram of a depth checkerboard with 8 × 6 checks (each 3.5° square) (Figure 2). The disparities of the checks were randomly distributed between near 0.22° and far 0.22°. The checks appeared to move at 2.2°/s when viewed binocularly, changing direction every 2 s. Through either eye alone, the stimulus consisted only of continuous random dot flicker at 15 Hz. We used the moving checkerboard in order to provide as rich a stereoscopic stimulus as possible. In further control experiments, we specifically tested the possibility that the activations elicited by this stimulus were due to segmentation (see Figures 8 and 9).

In selected experiments, the monkeys were given an injection of the magnetic contrast agent MION (monocrystalline iron oxide nanospheres) to increase the signal/noise ratio (Shen et al., 1993; Vanduffel et al., 2001; Leite et al., 2002). MION was essential to obtain a sufficient signal-to-noise ratio at 1.5 T; at 3 T, we tested and

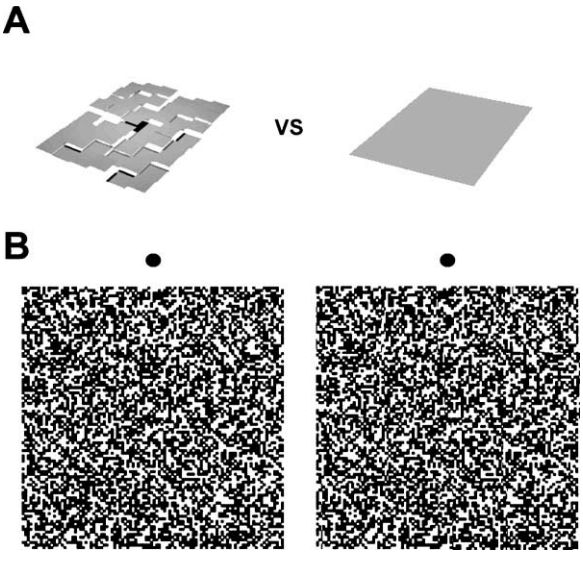

Figure 2. Overview of the Experimental Approach

(A) Schematic of the basic visual stimuli used in this study. A disparity-defined checkerboard alternated with a monocularly equivalent field of dots at zero disparity.

(B) A disparity-defined checkerboard pattern similar to that used in our experiment; it can be seen here by fusing the two dots.

found similar activation patterns with BOLD and MION imaging (see Supplemental Figure S2 at http://www.neuron.org/cgi/content/full/39/3/555/DC1, compare parts B and C with parts D and E). For ease of comparison and economy of space, all data are plotted on flat maps of macaque and human visual cortex (see Supplemental Figures S2 and S3 for representative slice data).

Figure 3 shows the pattern of activation to near/far versus zero disparity in four different monkeys. The red- and yellow-colored patches represent cortical regions that responded significantly more during the near/far disparity condition, compared to the zero disparity condition. Cortical regions that showed higher activity to the zero disparity condition are coded in blue-cyan; clearly, most activity was biased to the near/far stimulus. In all four monkeys, we found two main foci of activation: in the fundus and anterior bank of the lunate sulcus (areas V3 and V3A, respectively), and in the lateral, ventral bank of the caudal intraparietal sulcus (CIPS).

In Figures 3A and 3B, the area borders of early visual areas (outlined in blue) were obtained using meridian mapping (Vanduffel et al., 2002). In Figures 3C and 3D, area borders were determined by registering a surface-based atlas (Van Essen, 2003) onto the individual hemisphere, using the Lewis and Van Essen (2000b) partitioning scheme for parietal areas and the Ungerleider and Desimone (1986) partitioning scheme for temporal areas. In particular, Lewis and Van Essen (2000b) identified a region in the caudal intraparietal sulcus whose cytoarchitecture was distinct from adjacent areas V3A and LIP. They designated this region the "LOP zone." Here, we use the borders of the LOP zone to define area CIPS.

We confirmed the ability of one monkey (Figure 3C) to see stereo inside the scanner using a behavioral task. The animal was trained to signal the orientation change of a disparity-defined bar (monocularly invisible) for a juice reward. The monkey mastered this task within one scan session, achieving performance levels >95% while being scanned (this stereo task was very similar to a luminance-defined bar-orientation task the monkey already knew). Thus, the monkey was clearly able to perceive depth in random-dot stereograms inside the scanner. Prior to scanning, all human subjects affirmed their ability to see depth in the stereoscopic stimuli.

Figure 4 shows areas activated by near/far compared to zero disparity (same stimulus as in Figure 3) in four human subjects. In all four subjects, the strongest activity occurred in areas V3A (as in the macaque) and additionally in areas V4d-topo, V7, and CPDR. There was moderate activity in MT+, but this varied among subjects. For instance, in Figures 4A, 4B, and 4D, MT+ was only marginally activated, whereas in Figure 4C, MT+ was strongly activated. The borders of visual areas were determined through retinotopic mapping as well as additional functional criteria (see Experimental Procedures for details). The caudal parietal disparity region (CPDR) was defined as the region in the caudal human intraparietal sulcus that was activated by disparity compared to zero disparity with $p < 0.01$. We were forced to use this circular definition because there are no known independent functional tests that robustly parcellate this region of cortex.

In early human visual areas (V1, V2, V3/VP), disparity-related activation often occurred as an iso-eccentric band, accompanied by patches of suppression at other eccentricities (e.g., Figure 4B). This could reflect eccentricity-based variations in disparity tuning, since the dis-

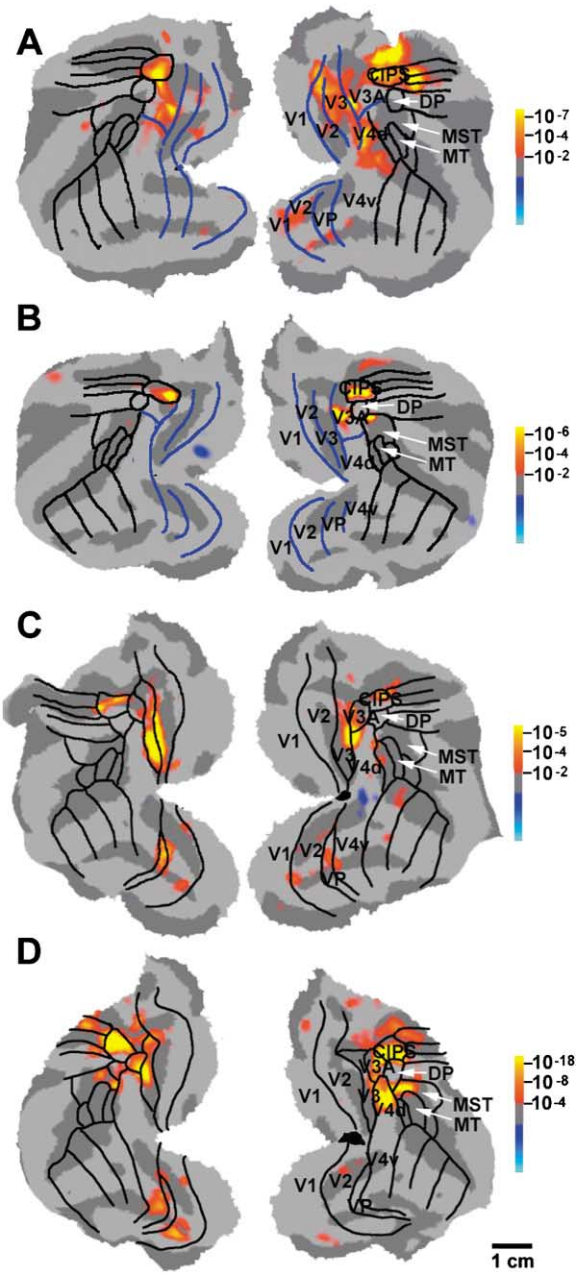

Figure 3. The Response to Near/Far Disparity was Strongest in V3, V3A, and CIPS in All Four Monkeys Tested

Differential activation maps obtained in response to a laterally moving disparity checkerboard that alternated with a zero disparity stimulus. Activation patterns from all four monkeys are overlaid on flat maps of the posterior 2/3 of cortex, which were derived from high-resolution anatomical scans of each monkey. In (A) and (B), scanning was done at 1.5 T using MION contrast agent and a simple fixation task. In (C) and (D), scanning was done at 3 T, using BOLD contrast and a foveal bar task. Supplemental Figure S6 at http://www.neuron.org/cgi/content/full/39/3/555/DC1 shows activation to the same stimulus, obtained from the monkey in (D), with scanning done at 3 T using MION contrast agent and a simple fixation task.

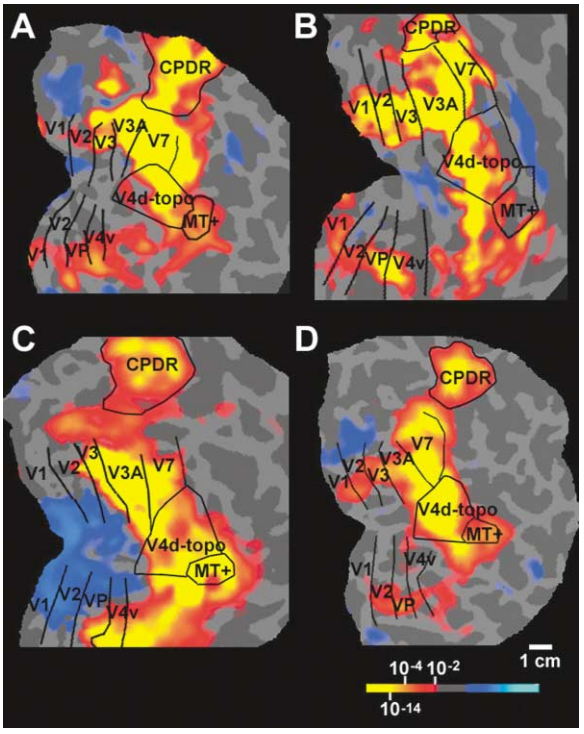

Figure 4. The Disparity Response Was Strongest in a Swath of Occipito-Parietal Areas Including V3A, V4d-topo, V7, and CPDR in Human Cortex

Stimuli were the same as in Figure 3. This figure shows cortical regions in four human subjects that responded more strongly to near/far compared to zero disparity. Due to space limitations, data from only one hemisphere is shown; to facilitate comparison, all data are shown in right hemisphere format. We consistently saw strong activity in V3A, V4d-topo, V7, and CPDR (a nonretinotopic region in the caudal IPS, dorsal to V7). In early visual areas (V1, V2, V3/VP), activation was patchy, often including isoeccentric bands accompanied by patches of suppression.

parity of each check was a randomly chosen value between near 0.22° and far 0.22°, independent of eccentricity, but the fusion limit is only 10 arcmin in the fovea (Crone and Leuridan, 1973). Alternatively, it could reflect global attention mechanisms, which can preferentially activate peripheral representations while suppressing foveal ones (Tootell et al., 1998b; Sasaki et al., 2001). In any case, the activity in these early human visual areas was statistically less significant than that in V3A, V4d-topo, V7, and CPDR.

In addition to the checkerboard, we also tested the response pattern to a disparity-defined annulus compared to zero disparity in both the macaque and the human (see Supplemental Figure S4 at http://www.neuron.org/cgi/content/full/39/3/555/DC1). The resulting BOLD activity was confined to areas V3 and CIPS, as with the disparity checkerboard stimulus (Figures 3 and 4), but it was weaker.

The intraparietal sulcus has been characterized as a visuomotor region involved in planning eye and arm movements (for review, see Mountcastle et al., 1975; Snyder et al., 2000). Thus, it is possible that the strong disparity activity in V3A and CIPS in macaques, and V3A and CPDR in humans, was an *indirect* consequence of increased conjugate and vergence eye movements during the disparity condition.

To test this possibility, in two monkeys, we tracked the eye movements (in one eye) during scanning. We did not find more horizontal or vertical eye movements during the disparity condition than during the zero disparity condition (F-test, horizontal position, $p < 0.28$; vertical position, $p < 0.39$). Moreover, we did not find a significant increase in activity in areas known to be activated prior to eye movements, such as the superior colliculus and LIP (Robinson, 1972; Gnadt and Mays, 1995), during disparity conditions (though this may have been due to limited sensitivity).

Finally, in one human subject, we explicitly imaged the BOLD activation to vergence eye movements compared to fixation (see Supplemental Figure S5 at http://www.neuron.org/cgi/content/full/39/3/555/DC1). In different blocks, a zero disparity fixation point alternated with a changing disparity fixation point (whose disparity spanned the same range as that used in the disparity checkerboard stimulus, ±0.22°). The subject was asked to track the changing disparity fixation point with vergence eye movements. This elicted two strong foci of activation in the anterior intraparietal sulcus and in the superior temporal gyrus, as well as a band of activation in foveal visual cortex (see Supplemental Figure S5A). For comparison, Supplemental Figure S5B shows the activation to the disparity checkerboard compared to zero disparity, obtained in interleaved scans in the same scan session as the vergence scans. Importantly, the overall activation pattern to vergence had almost no overlap with that to the disparity checkerboard stimulus, except in area V4d-topo. Furthermore, the "vergence" activation in V4d-topo was not necessarily due to vergence eye movements: V4d-topo is known to contain a foveally biased representation of the visual field (Tootell and Hadjikhani, 2001), and the changing disparity fixation point provided a powerful disparity stimulus in the fovea. Thus, several lines of evidence indicate that the disparity activations we observed were not due to vergence eye movements.

To compare activity in humans and macaques across visual areas more quantitatively, Figure 5 shows a bar graph of average disparity activation across different areas of the macaque (Figure 5A) and human (Figure 5B). Data are averages from four macaques and four human subjects (these four human subjects had the clearest retinotopy). In the macaque, strongest activation occurred in areas V3, V3A, and CIPS. In the human, strongest activation occurred in V3A, V7, V4d-topo, and CPDR. Thus, in both primate species, strong activity occurred in V3A. However, several interspecies differences were also apparent. (1) Humans showed strongest disparity activity in area V4d-topo, whereas macaques showed strongest disparity activity in CIPS. (2) Macaques showed strong disparity activity in area V3, while humans did not. (3) Humans showed some activity in MT, while macaques showed very little activity in MT. (4) Humans showed activity in area V7, a visual area without any certain macaque counterpart.

Figure 6 presents time courses from different visual areas in one macaque and one human subject. The three-condition stimulus used here (Figure 6A) included epochs of spatially uniform gray (of mean luminance

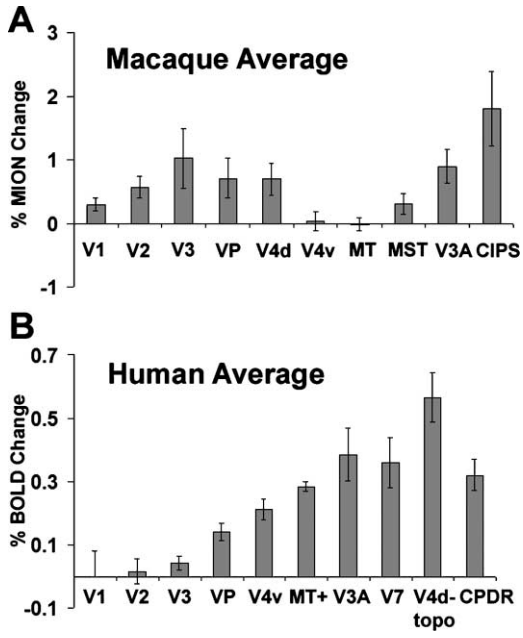

Figure 5. Quantitative Comparison of Average Disparity Activation in Different Visual Areas of Macaque and Human Subjects

(A) Percent signal changes in response to near/far versus zero disparity, averaged across both hemispheres of four monkeys.

(B) Percent signal changes in response to the same stimulus, averaged across both hemispheres of the four human subjects with the clearest retinotopy. Each bracketed line indicates one standard error. In both species, V3A was strongly activated.

equal to that of the random-dot stimuli), zero disparity, and a near/far disparity checkerboard.

In both subjects, area V1 responded strongly to *both* near/far disparity and zero disparity conditions, while areas V3, V3A, V4v, V4d, and CIPS in the macaque and V3A, V4d-topo, and V7 in the human responded more strongly to near/far disparity than to zero disparity. The time course from macaque CIPS was especially remarkable, showing almost no response to zero disparity at all.

Response to Coherently Moving Disparity

Human MT+ showed some disparity-enhanced response, whereas macaque MT did not (Figures 3–6). Given the large body of single-unit data that has been collected on disparity processing in macaque MT (Maunsell and Van Essen, 1983; Bradley and Andersen, 1998; Bradley et al., 1998; DeAngelis et al., 1998; DeAngelis and Newsome, 1999; DeAngelis and Uka, 2003), we were surprised at the lack of fMRI activity to disparity in macaque MT.

One possibility is that disparity modulation in MT requires *coherently moving* patterns (in Figures 3–6, the disparity stimulus consisted of random flicker without any coherent motion when viewed monocularly). To test this, we presented a three-condition stimulus, consisting of (1) static zero disparity, (2) moving zero disparity, and (3) a moving disparity checkerboard (Figure 7A). Both the moving zero disparity stimulus and the moving disparity checkerboard were generated with a random-dot pattern that moved coherently within each eye at 2.2°/s, changing from leftward to rightward motion every two seconds.

In the macaque, only area MT was significantly activated by the comparison of moving zero disparity versus static zero disparity (Figure 7B). This confirmed the motion sensitivity of area MT (Vanduffel et al., 2001). However, for the comparison between the moving disparity checkerboard and the moving zero disparity stimulus, V3A and CIPS were activated, but *not* MT (Figure 7C). Thus, the negative result in macaque MT was *not* due to a lack of coherent monocular motion in the disparity checkerboard. The positive result in V3A and CIPS confirmed the robust stereo selectivity of these areas. Figure 7D shows time courses obtained from V1, V3A, CIPS, and MT.

Binocular Uncorrelation

A binocularly uncorrelated stimulus yields the percept of a 3D cloud of dots at different depths, but unlike the checkerboard stimulus, lacks surface structure (Julesz, 1971). Figures 8A and 8B plot the response magnitude across macaque and human visual areas, respectively, to a string of five stimuli, consisting of (full screen) zero disparity, disparity checkerboard, binocularly uncorrelated random-dot pattern, and a monocular random-dot pattern. In comparison to the zero disparity stimulus, the uncorrelated stimulus elicited weaker activations across most macaque visual areas, but stronger activations across most human visual areas. But in almost all areas of both macaque and human visual cortex, the response to the binocularly uncorrelated stimulus was weaker than that to the disparity checkerboard stimulus. This suggests the importance of cooperative surface-based interactions across all tiers of the visual system.

The reason why activation in V3A appears less significant in Figure 8A compared to Figure 5A is that the bar graph in Figure 5A was derived from 16 times as much data as that in Figure 8A. Figure 8A is based on data from two monkeys, while Figure 5A is based on data from four monkeys. Furthermore, in the experiment for Figure 8A, we tested four different conditions with blank epochs interleaved between each of the four conditions to mitigate order effects, while in Figure 5A we tested only two conditions.

Absolute versus Relative Disparity

Disparity can be described in terms of absolute disparity (disparity relative to the fixation point) or relative disparity (disparity relative to that at a nearby location). The disparity checkerboard contained a greater range of absolute as well as relative disparities compared to the zero disparity stimulus. Thus, the maps in Figures 3 and 4 presumably imaged areas processing either/both type(s) of disparity. To isolate areas activated by each type of disparity, we presented a three-condition stimulus, consisting of zero disparity, full screen moving in and out, and disparity checkerboard with individual checks moving in and out (each through the same range as in the full screen condition, ± 0.22). In Figure 8C, the left map shows activation in a macaque subject to the full screen moving in and out versus zero disparity (absolute disparity), while the right map shows activation to the disparity checkerboard versus the full screen moving

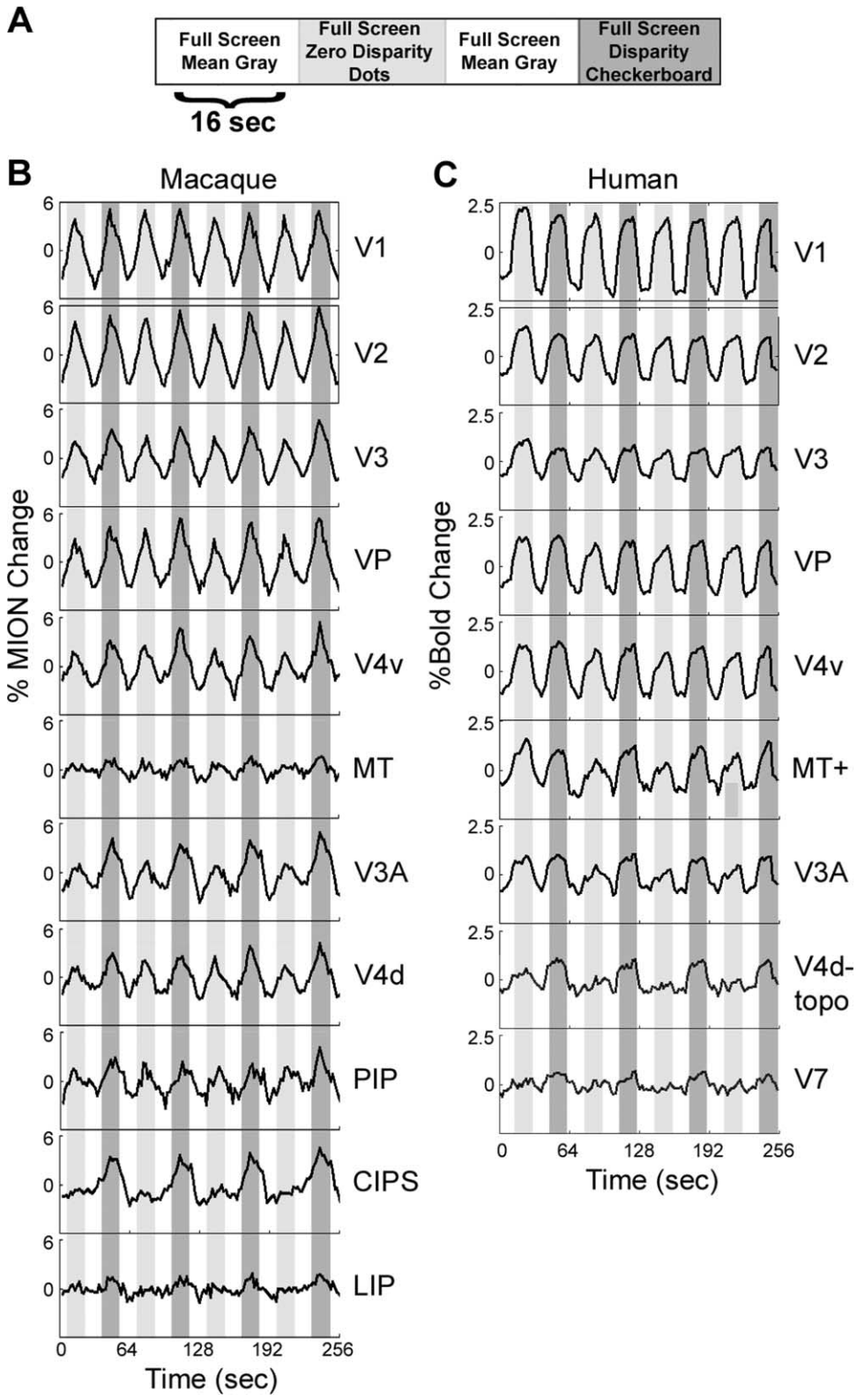

Figure 6. Time Course of fMRI Responses to Disparity in Macaque and Human

(A) A schematic of the stimulus sequence.

(B and C) Time courses in monkey and human, respectively, generated by computing the average time series over all voxels in a given visual area. The monkey time courses (B) look more triangular-wave-shaped than the human time courses (C) because MION has a slower time course than conventional BOLD responses (Vanduffel et al., 2001; Leite et al., 2002). The time courses have all been shifted 4 s relative to the stimulus to accommodate the hemodynamic delay. Similar time courses were obtained using BOLD (see Supplemental Figure S1 at http://www.neuron.org/cgi/content/full/39/3/555/DC1).

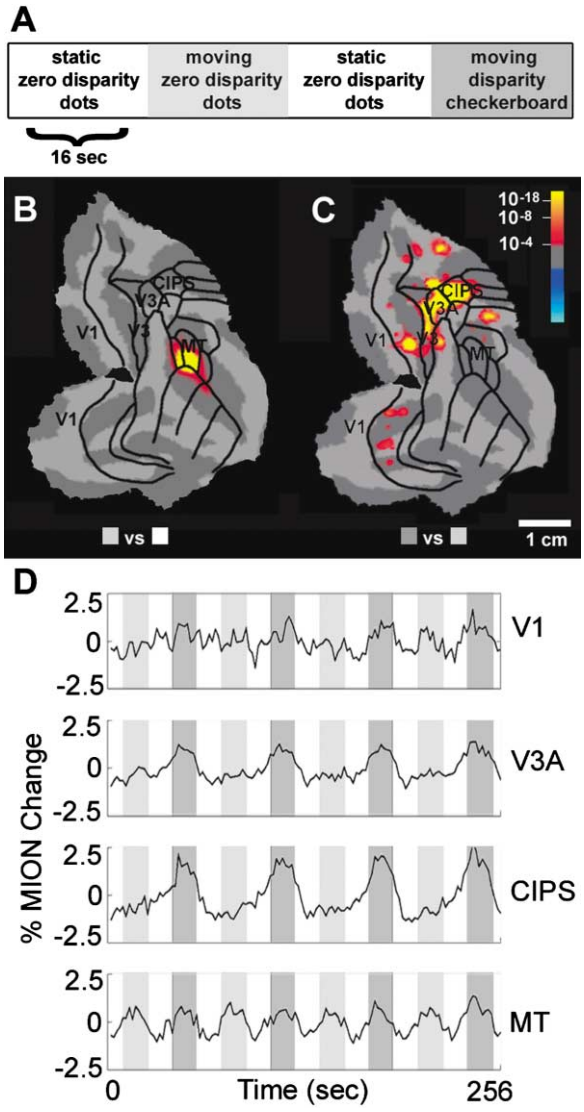

Figure 7. The Response to a Coherently Moving Disparity Pattern in Macaque MT and V3A/CIPS

Coherent global motion was visible in the monocular carrier. MION contrast agent was used.

(A) A diagram of the three-condition (A-B-A-C) stimulus, where A = static zero disparity, B = moving zero disparity, and C = moving disparity checkerboard. The random-dot pattern moved at 2.2°/s and reversed direction (left to right) every 2 s.

(B) Areas that were more activated by the moving zero disparity condition than by the static zero disparity condition; MT was the only area significantly activated by this classic moving-versus-stationary test.

(C) Areas that were more activated by the moving disparity checkerboard condition than by the moving zero disparity condition; in this comparison, V3A and CIPS were the only areas showing significant activation.

(D) Response time courses from V1, V3A, CIPS, and MT. The time course from MT shows that it was more sensitive to motion than to disparity.

in and out (relative disparity). Surprisingly, the absolute disparity stimulus elicited strongest activation in V3, MST, and MT/FST, while the relative disparity stimulus elicited strongest activation in V3A and CIPS. Similar patterns were obtained in three additional hemispheres (data not shown). Thus, it appears that MT does not respond well to an edge-rich disparity pattern but prefers large disparity patterns coherently changing in depth.

Figure 8D shows activation in response to the same two stimulus comparisons in a human subject. Early visual areas, as well as ventral areas including the lateral occipital complex anterior to V4v, were activated by the relative disparity stimulus but not by the absolute disparity stimulus. These areas appear to be involved in disparity-based segmentation processes. V3A, V4d-topo, and V7 were activated by both relative and absolute disparity, while MT+ (as in the macaque) and CPDR were activated only by absolute disparity.

Because the size of the checks within the checkerboard stimulus was not systematically varied, it is possible that the above test for relative disparity representations may have missed regions in which the average receptive field size is smaller than the size of the checks. In such areas, the checkerboard stimulus would have provided mainly absolute disparity variations.

Attention

Many of the areas activated by disparity have also been reported to be activated by attention in other studies (Corbetta et al., 1998; Le et al., 1998; Tootell et al., 1998b; Wojciulik and Kanwisher, 1999). It is likely that attention interacts with disparity processing, since one purpose of attention is to select useful objects out of a cluttered environment, and disparity is one of the primary cues to detect depth edges and object boundaries.

Nevertheless, the disparity-driven activation we observed in macaque and human subjects was not simply due to increased attention. In both the monkey and the human, the overall topography of activation to near/far versus zero disparity was similar, regardless of whether the subject was performing an attention-demanding bar-orientation detection task or a passive fixation task. If one assumes a "capacity limitation" to visual spatial attention, then this indicates that disparity-driven activation was not due solely to attention (Kastner et al., 1998; Gandhi et al., 1999; Somers et al., 1999).

Figure 3D shows disparity-driven activation from a monkey performing the foveal bar task; Supplemental Figure S6 (at http://www.neuron.org/cgi/content/full/39/3/555/DC1) shows activation from the same monkey performing a simple fixation task. The activation patterns were similar: strongest activation occurred in areas V3, V3A, and CIPS.

Likewise, in a human subject who performed both the passive fixation task (Figure 8E, left) and the bar-orientation discrimination task (Figure 8E, right), the overall topography of activation was similar. V3A, V4d-topo, CIPS, and V7 were all significantly activated during performance of both the passive fixation and the attention-demanding task. However, the amplitude of the MR signal was somewhat diminished, especially in higher areas (MT, V7, V4d-topo, CIPS) during the bar task (Figure 8F), suggesting that disparity processing in these areas may be modulated by attention.

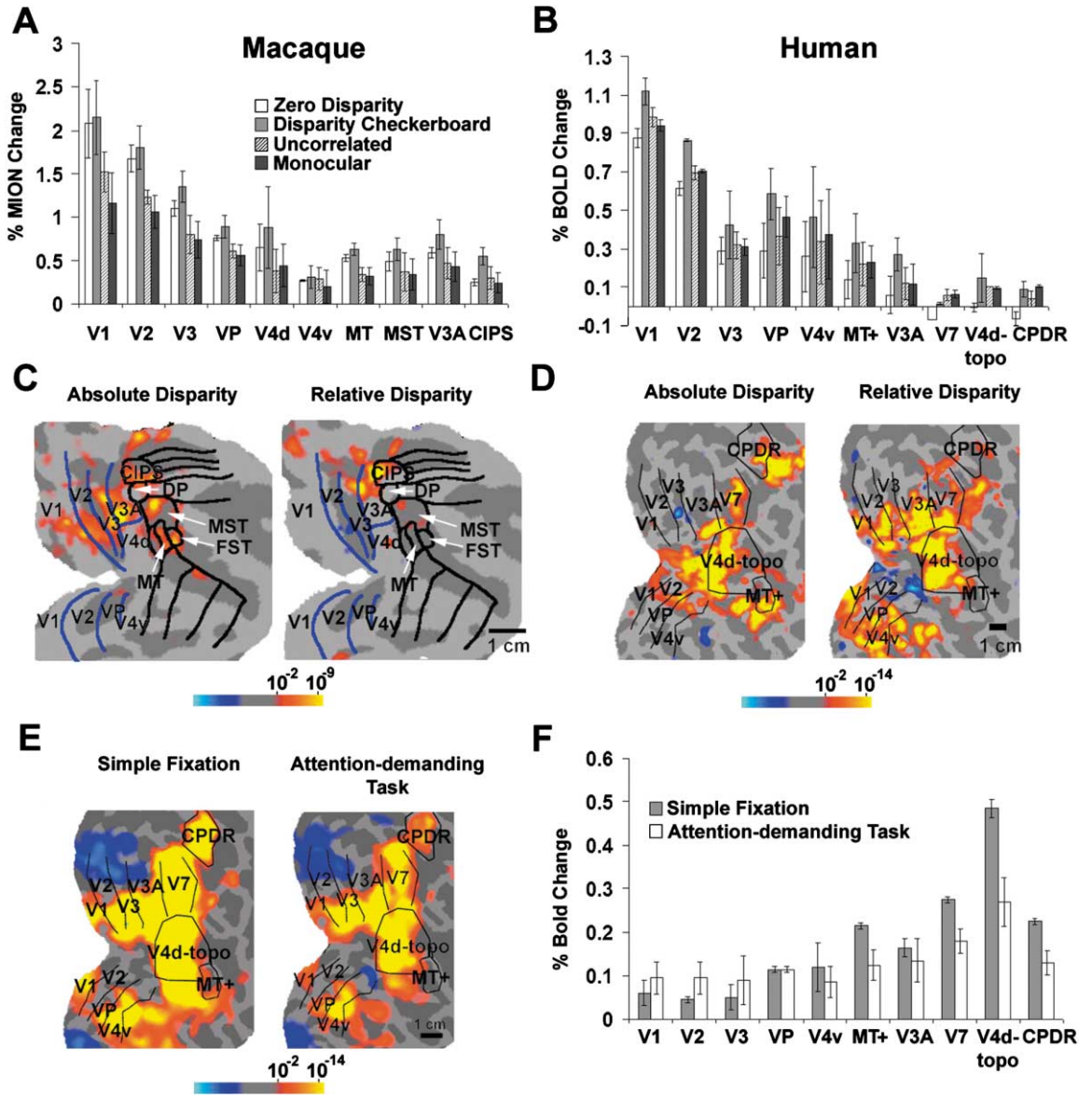

Figure 8. Additional Controls Clarifying the Nature of Disparity-Driven fMRI Activity: The Response to Binocular Uncorrelation, Relative versus Absolute Disparity, and Attention

(A and B) Bar graphs comparing the response to zero disparity, disparity checkerboard, binocular uncorrelation, and a monocular pattern, in both the macaque and human. Responses to a left eye monocular pattern and a right eye monocular pattern were averaged. All patterns were presented via a full-field 15 Hz refresh random-dot carrier. Data represent averages of two macaque subjects and two human hemispheres.

(C and D) Absolute and relative disparity maps in the macaque (C) and human (D). In response to a three-condition stimulus (zero disparity, full screen moving in and out, and disparity checkerboard), the left maps show areas activated by the full screen moving in and out compared to zero disparity, while the right maps show areas activated by the disparity checkerboard compared to the full screen moving in and out. MION contrast agent was used in (A) and (C).

(E) Activity maps obtained during simple fixation (left) as well as during performance of an attentionally demanding foveal bar task (right), in the human. The two types of task were interleaved within the same scan session.

(F) Quantification of the decrease in disparity activation in higher areas when attention is distracted.

Segmentation versus Disparity

Disparity is a powerful cue to scene segmentation. For example, in the stereogram in Figure 2B one can perceive numerous square shapes. The sensitivity to relative disparity in macaque areas V3A and CIPS (Figure 8C) and human areas V3A, V7, and V4d-topo (Figure 8D) indicates that these areas are not just sensing absolute disparities, but are also computing the locations of disparity-defined edges. To test whether these areas have a general role in scene segmentation or whether they are specialized for 3D scene segmentation specifically, we mapped the response to an *orientation*-defined checkerboard pattern, compared to a uniform-orientation pattern.

Figure 9A shows the activation maps in a macaque and human subject to an orientation-defined checker-

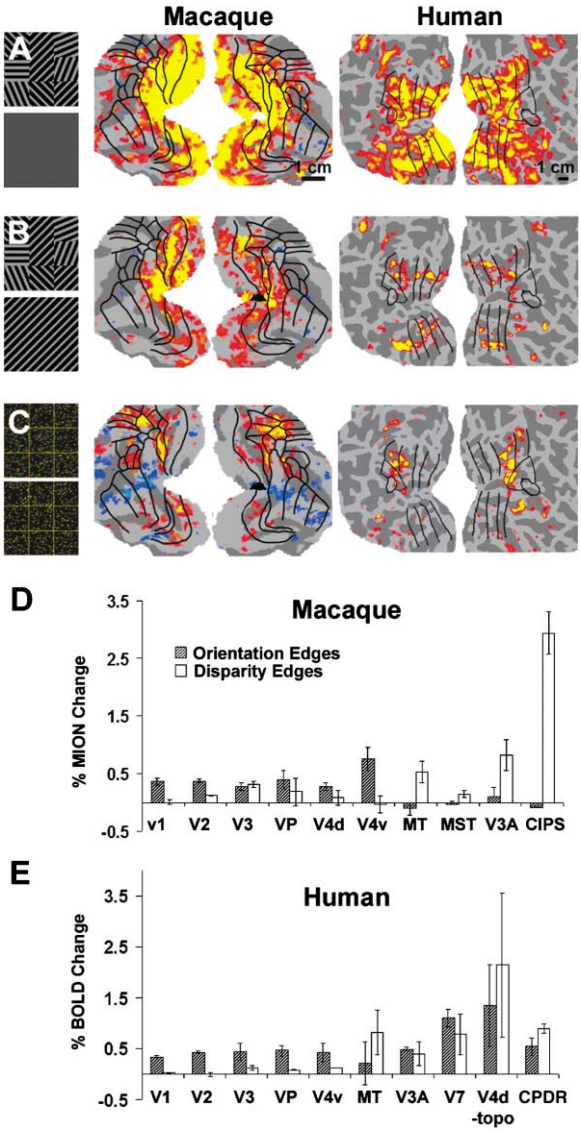

Figure 9. Disparity-Based Segmentation versus General-Purpose Segmentation

(A–C) Left and right hemisphere activity maps in the macaque and human to (A) an orientation-defined checkerboard versus uniform-luminance gray, (B) an orientation-defined checkerboard versus a uniform-orientation pattern, and (C) a disparity checkerboard versus zero disparity, with a zero disparity grid visible during both conditions.

(D and E) Bar graphs quantifying the activation to disparity and orientation-defined edges across visual areas of the macaque and human, respectively. Data represent averages of two macaque and two human subjects. Orientation edges activated lower-tier visual areas more strongly than disparity edges in both species. MION contrast agent was used for the monkey experiments.

board versus uniform mean gray. This stimulus activated a large number of visual areas including V3, V3A, and CIPS (weakly) in the macaque, and V3A, V7, V4d-topo, and CPDR in the human. Figure 9B (left) shows the activation map in a macaque to the orientation-defined checkerboard versus the uniform-orientation pattern. This produced strong activation in V1, V2, and V4; weak activation in V3; and no activation in V3A and CIPS. Thus, V3A and CIPS are not concerned with general-purpose scene segmentation. In the human (Figure 9B, right), the orientation-defined checkerboard also produced more activation in early visual areas than the disparity checkerboard.

Finally, we compared the response to a disparity checkerboard with that to zero disparity, as in Figures 3 and 4—but now with a zero disparity grid superimposed on both the checkerboard and the zero disparity patterns. This stimulus should equate the scene segmentation processes stimulated by the two patterns. Nevertheless, we observed significant activation in V3, V3A, and CIPS in the macaque, and in V3A, V7, V4d-topo, and CPDR in the human (Figure 9C). This further demonstrates that these areas are not simply segmenting the scene into different shapes, but are processing the 3D layout.

Discussion

In both humans and monkeys, lesions to the posterior parietal lobe can cause profound deficits in spatial awareness, including neglect of the contralateral half of visual space, inability to draw simple 3D objects such as a cube, and inability to estimate distance and size (for review, see Thier and Karnath, 1997). These observations suggest that the posterior parietal lobe is crucial to cortical 3D processing. Here, our fMRI results confirm that a specialization for 3D processing exists in the posterior parietal lobe in both humans and monkeys. Binocular disparity produced the highest levels of fMRI activity in only a small cluster of areas in the dorsal stream: V3, V3A, and CIPS in the monkey, and V3A, CPDR, V7, and V4d-topo in the human.

These results raise at least three questions. (1) What is the functional correlate of the disparity fMRI signal (e.g., absolute versus relative disparity, attention, eye movements, etc.)? (2) How does the pattern of disparity-based fMRI activity in monkeys compare to results from single units? (3) How does the architecture of disparity processing in monkeys compare to that in humans?

What Is the Source of the Disparity-Related fMRI Signal?

There are at least four possibilities. (1) Increased fMRI activity to near/far compared to zero disparity could reflect the concentration of near and far disparity-tuned cells in a region. (2) The activity could reflect the processing of relative disparity signals and/or high-level shape extraction. (3) The activity could be due to secondary planning and execution of eye movements elicited by the disparity stimulus. (4) The activity could be caused by a general increase in attention during the near/far disparity condition compared to the zero disparity condition.

The last two possibilities appear unlikely. Monitoring of eye movements inside the scanner indicated no difference in the magnitude of horizontal or vertical eye movements during near/far compared to the zero disparity conditions. Furthermore, explicit imaging of activity produced by vergence eye movements showed that vergence eye movements and stereoscopic surfaces activated largely nonoverlapping regions of cortex (see

Supplemental Figure S5 at http://www.neuron.org/cgi/content/full/39/3/555/DC1). However, we cannot rule out the possibility that eye movement differences between the disparity-rich and zero disparity conditions contributed to some of the activation patterns we observed.

It is also unlikely that apparent disparity sensitivity was due solely to increased attention (possibility 4 above). In the human, disparity-driven activation was weaker when attention was diverted by a demanding foveal task (Figures 8E and 8F). Nevertheless, in both the monkey and the human, the overall topographic pattern of activity produced when the subject performed a difficult bar-orientation discrimination task during disparity scanning was similar to that obtained when the subject performed a passive fixation task (macaque, Figure 3D and Supplemental Figure S6; human, Figure 8E).

This leaves the first two possibilities: near/far cells and/or cells sensitive to relative disparity produced the disparity-driven fMRI activity. The results of the relative disparity experiment (Figures 8C and 8D) indicate that disparity activation in macaque areas V3, V3A, and CIPS and human areas V3A, V7, and V4d-topo was most likely due to a combination of both absolute and relative disparity processing (possibilities 1 and 2), while disparity activation in macaque area MT and in human areas MT+ and CPDR was due to absolute disparity processing. Furthermore, relative disparity activity in macaque areas V3, V3A, and CIPS was not due to general scene segmentation processes, but was due to 3D scene segmentation specifically, since we found no activation in these areas to an orientation-defined checkerboard versus a uniform-orientation pattern (Figure 9B).

How Does Disparity fMRI Activity in Monkeys Compare to Results from Single-Unit Recordings in Monkeys?

Disparity-tuned cells have been found in almost every cortical visual area, yet the pattern of fMRI activity was much more localized. Direct comparison of monkey fMRI results with single-unit results is difficult. Within each voxel, fMRI samples averaged activity across hundreds of thousands of neurons via hemodynamics. Depending on the size of functional domains relative to the voxel size, activity within single cells could be modulated by disparity, yet activity within single fMRI voxels could remain unchanged. For example, if an area contained equal numbers of near, far, and zero disparity-tuned cells, randomly scattered, then the net activity of an fMRI voxel in this area to the near/far checkerboard stimulus and the zero disparity stimulus would be the same. This may explain why we did not see differential fMRI activity in areas V1 and V2 to the disparity checkerboard stimulus compared to the zero disparity stimulus.

Our strongest disparity activations occurred in areas V3, V3A, and CIPS. Although existing evidence is sparse, single-unit studies suggest that these three areas could indeed be rich in near and far disparity-tuned cells. Poggio et al. (1988) reported that 80% of the cells in V3/V3A are disparity tuned. Moreover, several researchers have found disparity columns in V3/V3A (Hubel and Wiesel, 1970; Adams and Zeki, 2001; D.Y.T., unpublished observations).

Area CIPS lies adjacent to V3A, at the junction of the lunate and intraparietal sulci, and it receives strong inputs from V3A (Nakamura et al., 2001). This relatively unexplored cortical area has a distinctive cytoarchitecture, and has been designated the "LOP zone" by Lewis and Van Essen (2000a). The strong, circumscribed disparity-related fMRI activity in CIPS (which did not spread more anteriorly to LIP) supports the elevation of CIPS from a "zone" to a full-fledged area. Sakata et al. (1998) found that cells in CIPS are tuned to the orientation of 3D surfaces defined by stereo and/or perspective. We found strong activation in CIPS to the disparity checkerboard stimulus even though it had the same frontoparallel orientation as the zero disparity stimulus everywhere. This suggests that CIPS may process not only surface orientation, but also other surface parameters such as depth edges.

Several groups have reported disparity-tuned neurons in V4 (Watanabe et al., 2000; Hinkle and Connor, 2000). Here we found the strongest disparity fMRI activity in areas V3, V3A, and CIPS, but there was disparity-specific activity in V4d and V4v as well.

Both MT and MST contain disparity-selective neurons (Maunsell and Van Essen, 1983; Roy et al., 1992; Bradley and Andersen, 1998; DeAngelis and Uka, 2003). In MT, DeAngelis and Newsome (1999) observed a system of near and far disparity columns and showed that microstimulation of single columns could affect the monkey's percept of depth in predictable ways (DeAngelis et al., 1998).

Here, we found that MT was not activated by the disparity checkerboard compared to zero disparity, but it was activated by the changing disparity plane compared to zero disparity (Figure 8C). This suggests that MT is not important for detection of disparity edges.

It is difficult to reconcile this with the report by Bradley and Andersen (1998) that 52% of MT cells were significantly modulated by the disparity in the nonclassical receptive field surround, and the center-surround interaction was usually antagonistic. One would expect cells with antagonistic disparity surrounds to respond better to a disparity checkerboard than to a zero disparity stimulus.

At the very least, the strong relative disparity activations in areas V3, V3A, and CIPS (Figure 8C, right) suggest these latter areas may be *more* important than MT for disparity edge representations. Why might V3, V3A, and CIPS contain more disparity edge detectors than MT? One possibility is that V3, V3A, and CIPS are involved in encoding 3D shape, while MT primarily encodes motion in 3D space. In this model, binocular disparity would be a critical stimulus parameter for all three areas, but it would be used for different purposes in each area. In MT, disparity information would reinforce depth relationships constructed from motion parallax (Xiao et al., 1997; Orban et al., 1999; Vanduffel et al., 2002) and would aid in separating motion vectors to different depth planes during transparent motion perception (Bradley et al., 1998) (however, see Peuskens et al., 2002, for evidence that human MT+ may be involved in 3D shape processing per se). Since the *motion* of the disparity checkerboard stimulus is the same as that of the zero disparity stimulus (both stimuli drift laterally at 2.2°/s), MT would be activated similarly by both

stimuli. In V3, V3A, and CIPS, on the other hand, disparity information would be used to reconstruct the 3D shape of an object. A disparity checkerboard has a more complex shape than a flat panel of zero disparity dots, and hence it would activate V3, V3A, and CIPS better. Alternatively, V3, V3A, and CIPS may be involved in processing global 3D layout, and disparity-defined object shape may instead be computed in the ventral stream. Janssen et al. (2000) have shown that neurons in the lower bank of the STS in area TE are exquisitely sensitive to disparity-defined curvature.

Comparison of Disparity Activity in Monkey and Man

Humans and macaques have evolved independently of each other for over thirty million years. Thus, it is unlikely that there exists a one-to-one homology between all cortical areas in the two species (e.g., Allman, 1999; Krubitzer, 2000). The current results corroborate this view and underscore the importance of doing fMRI in monkeys rather than in humans, if one's goal is to obtain an activity map to guide single-unit studies. In both species, V3A was activated by disparity. But the distribution of disparity activity was different in the two species: the strongest disparity activation occurred in area CIPS in macaques and in the V4d topolog in humans.

The disparity sensitivity in area V3A, common to both humans and monkeys, is interesting from an evolutionary perspective. Although human and macaque V3A are topographically homologous and have a similar retinotopy (both contain a contiguous representation of the entire contralateral visual field), an important functional difference exists between them: human V3A is moderately motion sensitive (Tootell et al., 1997), whereas macaque V3A is not (Zeki, 1978; Gaska et al., 1988; Galletti et al., 1990; Vanduffel et al., 2001). The finding here that both human and macaque V3A are disparity selective suggests that stereopsis may be a more evolutionarily fundamental function of area V3A, compared to motion processing.

The activation patterns to stereoscopic stimuli that we have observed in the macaque brain strongly emphasize the importance of areas V3, V3A, and CIPS in 3D processing. They provide single-unit physiologists with a new roadmap, and detailed physiological study of these areas may reveal the circuits by which single cells and groups of cells generate the percept of surfaces in space.

Experimental Procedures

General experimental details are similar to those described elsewhere for humans (Sereno et al., 1995; Tootell et al., 1997, 1998a; Hadjikhani et al., 1998) and for monkeys (Vanduffel et al., 2001; Leite et al., 2002). Supplemental Table S1 at http://www.neuron.org/cgi/content/full/39/3/555/DC1 lists the number of subjects used for the experiments in each figure.

Subjects

Monkeys

Four male macaque monkeys, 2–4 kg in weight, were used. Two monkeys were scanned in Belgium (Vanduffel et al., 2001) on a 1.5 T scanner (Siemens Vision), and two were scanned at MGH, on a 3 T scanner (Siemens Allegra). In order to motivate them to work (fixate) in the scanner, the monkeys had restricted access to water in their cages. They were given a regular ration of biscuits, and had free access to fruits and water at least once per week. Each animal was typically scanned three times a week. All procedures conformed to local, National Institutes of Health, and European guidelines for the care and use of laboratory animals.

Humans

Eight human subjects took part in this study. All human scanning was done at MGH, in the 3 T scanner. Informed written consent was obtained from each subject prior to each scan session, and all procedures were approved by Massachusetts General Hospital Human Studies Protocol #001155. All subjects had normal or corrected-to-normal vision.

Monkey Surgery and Training

During the three weeks prior to surgery, the monkeys were trained to jump into the chair for a juice and fruit reward. The chair designs used in Belgium and MGH were slightly different, but both restrained the monkey in the so-called sphinx position (head facing forward inside the horizontal bore). The chair used at MGH was purchased from Primatrix (Melrose, MA). Following initial chair training, each monkey was implanted with a MR-compatible plastic headset attached to the skull by plastic T-shaped anchors and ceramic screws (see Vanduffel et al., 2001, for surgery details).

Visual Task

All four monkeys were trained to optimal performance on a high-acuity bar-orientation discrimination task. In this task, a small bar was presented at the center of the visual display. The orientation of the bar changed from vertical to horizontal at a random time between 1 and 3 s after the start of a trial, and the monkey had to signal the orientation change within 500 ms for a juice reward (see Vanduffel et al., 2001, and Leite et al., 2002, for details).

In addition, all four monkeys were trained to fixate using direct monitoring of eye movements inside the scanner with a pupil/corneal reflection tracking system (RK-726PCI, Iscan Inc., Cambridge, MA). The monkey was rewarded with drops of apple juice for maintaining fixation within a square-shaped central fixation window (2° on a side). On average, during scanning, the monkey's eye was within the fixation window 92% of the time.

MION Injections

For details on MION injections and the relationship between the MION and BOLD signal, see Vanduffel et al. (2001) and Leite et al. (2002). For contrast agent-based experiments, MION (8–10 mg/kg), diluted in 2 ml of a sodium citrate buffer, was injected intravenously into the femoral vein below the knee. MION time courses have been inverted to facilitate comparison with BOLD time courses.

Visual Stimuli

Visual stimuli were projected from a Sharp XG-NV6XU or Barco 6300 LCD projector (640 × 480 pixels, 60 Hz refresh rate) onto a screen that was positioned 53 cm (MGH) or 54 cm (Belgium) in front of the monkey's eyes, or 42 cm in front of the human's eyes. The display spanned 28° laterally and 21° vertically (monkeys, MGH). Visual stimuli were generated on a Silicon Graphics O2. During simple fixation experiments, a tiny fixation cross (0.2° × 0.07°, each leg) was presented at the center of the screen. During experiments in which fixation was engaged through the foveal bar task, a tiny bar (0.2° × 0.09°) was presented over a small black square mask (0.4° side length) located in the center of the screen.

All stimuli were presented in a block design. Each scan typically lasted 4 min 16 s. Two-condition (A-B) stimulus comparisons were presented for 16 s/condition and 8 cycles per scan. Three-condition (A-B-A-C) stimulus comparisons were presented for 16 s/condition and 4 cycles per scan.

In all stereograms, the dot density was 5%, and each dot was 0.09° × 0.09°. The luminance of the red dots through the red filter was 10.6 cd/m^2; through the green filter it was 0.0 cd/m^2. The luminance of the green dots through the green filter was 23.8 cd/m^2; through the red filter it was 0.36 cd/m^2.

Magnetic Resonance Imaging

Monkeys

A total of 112,460 functional monkey brain volumes were acquired for the experiments described here. Scanning procedures were simi-

lar for the two scanners; the following details pertain specifically to the Siemens 3 T Allegra (details for the 1.5 T scanning are described in Vanduffel et al., 2001). A custom send/receive surface coil was used. Each monkey scan session lasted for about 3 hr. Each experiment began with a scan that served as input to an online optimization procedure for calculating shim coil settings. After shim coils were adjusted, a three-slice scout was taken to localize the brain. The monkey's head was arranged to be in the center of subsequent MR images, to increase signal and decrease distortion. Then a series of a T1-EPI's (21 slices; 1.72 × 1.72 × 2 mm voxels; no gap) were collected, which were used to register the functional data to the high-resolution anatomy. This was followed by 20–40 functional scans, each lasting 4 min 16 s (EPI; TR = 2 s; TE = 30 ms; 64 × 64 matrix; 1.72 × 1.72 × 2 mm voxels; 21 coronal slices). In a separate scan session, the high-resolution anatomy was obtained while the monkey was anesthetized with ketamine (10 mg/kg; Ketaset, Fort Dodge Labratories) (3D-MPRAGE; 256 × 256 matrix; 128 slices; 1 × 1 × 1 mm voxel size).

Humans

A total of 24,960 functional volumes of the human brain were acquired in this study. Images were acquired using a bilateral quadrature receive-only surface coil, molded for relatively uniform sensitivity throughout occipital cortex, including posterior portions of temporal and parietal cortex. The scan procedure was otherwise similar to that for monkeys. Each session began with a sagittal localizer to ensure proper head positioning. This was followed by a 3D-MPRAGE sequence used to localize the calcarine sulcus. The first echo-planar scan was a T1-weighted inversion recovery scan (21 slices; 3.1 × 3.1 × 3.1 mm voxels; no gap) used to align subsequent functional scans to the cortical surface. Slices were oriented in an oblique axial plane, approximately perpendicular to the calcarine sulcus. This was followed by 6–10 functional scans, each lasting 4 min 16 s (EPI; TR = 2000 ms or 4000 ms; TE = 30 ms; 64 × 64 matrix; 3.1 × 3.1 × 3.1 mm; 21 slices). Structural MR images needed to reconstruct the cortical surface were acquired in a separate session (3D-MPRAGE; 1 × 1 × 1 mm) and were optimized for contrast between gray and white matter.

Cortical Flattening

The procedures used for reconstructing, inflating, and flattening human cortex have been described comprehensively elsewhere (Sereno et al., 1995; Dale et al., 1999; Fischl et al., 1999; also see http://www.nmr.mgh.harvard.edu/freesurfer). To flatten monkey cortex, we made a few minor adjustments to the procedure for human subjects. Specifically, we made the following modifications. (1) Before running the white matter region-growing algorithm, we manually selected several white matter "control points" in the occipital and temporal lobe, which the algorithm would automatically classify as white matter. This step was necessary because the contrast between gray and white matter is slightly lower in monkeys, and the white matter strands are thinner than in human cortex. (2) The automatic skull-stripping algorithm did not work, and therefore we had to manually erase the image components corresponding to the skull. Otherwise, all procedures for cortical flattening generalized from humans to monkeys.

Area Border Delineation

Monkeys

In two monkeys, area borders for early visual areas were obtained through meridian mapping (Vanduffel et al., 2002). In two additional monkeys, they were derived from a surface-based atlas (Van Essen, 2003) and were mapped to individual hemispheres by surface-based registration of spherical maps (Van Essen et al., 2001) using CARET software (atlases and software available via http://brainmap.wustl.edu).

Humans

Retinotopic maps were obtained from all eight subjects. The boundaries of retinotopic cortical areas (V1, V2, V3, VP, V3A, and V4v) were defined for each subject on the basis of phase-encoded retinotopy (Engel et al., 1997; Sereno et al., 1995; DeYoe et al., 1996; Tootell et al., 1997) and subsequent calculation of field sign boundaries (Sereno et al., 1995). Of these eight subjects, we used the four subjects showing the clearest retinotopy for our population anaylsis of disparity (Figure 5). In addition to classically retinotopic areas, we also drew borders for MT+, V7, V4d-topo, and CPDR.

Human MT+ was localized using a low-contrast motion stimulus (Tootell et al., 1995). V7 was identified as an area adjacent and anterior to V3A that contains a crude representation of at least the upper visual field, mirror-symmetric to that in V3A (Tootell et al., 1998b; Press et al., 2001). V4d-topo was identified as the human *topographic* homolog ("topolog") of macaque V4d, an area situated (1) superior to V4v, (2) anterior to V3A, and (3) posterior to MT+. It was called "LOC/LOP" in Tootell and Hadjikhani (2001). Here, we have renamed the area "V4d-topo" to avoid unnecessary confusion with LOc, the lateral occipital complex, which lies more ventral (Grill-Spector et al., 2001). Finally, human CPDR was defined as a region on the medial bank of posterior IPS, located superior to V7 on the flattened map, which responded to the disparity checkerboard versus zero disparity test with $p < 10^{-2}$.

Functional MR Data Analysis

Three main steps were applied to obtain activation maps like those shown in Figure 3: (1) motion correction, (2) generation of statistical maps for different stimulus comparisons, and (3) rendering statistical data onto the flattened occipital patch. The same steps were used for analyzing both human and monkey data.

Motion Correction

Despite physical fixation of the monkeys' heads in the restraint device, apparent brain motion and small distortions resulted from changes in the magnetic field associated with body motion. To minimize such effects, 3D motion correction was applied to all monkey and human data sets using the "AFNI" motion correction algorithm (Cox and Hyde, 1997).

Generation of Statistical Maps

To generate statistical maps, we used the MGH Standard Processing Stream (FS-FAST). This software first normalizes the images to correct for signal intensity changes and temporal drift. Then, at each voxel, averages of the normalized data are generated for each of the different conditions. From these averages, statistical activation maps are constructed using a t test. Activation maps were smoothed with a Gaussian smoothing kernel (human, 3 mm; monkey, 2 mm full width at half maximum).

Rendering Data onto Flattened Patches

At the beginning of each scan session, we took a T1-EPI data set with the exact same slice prescription (number, position, and orientation of slices) as in subsequent functional scans. By manual iterative alignment in three orthogonal planes between this T1-EPI data set and the high-resolution anatomy, we were able to register the functional data set to the flattened patch (see Mendola et al., 1999, for details).

Across-Subject Analysis

This analysis is shown in Figures 5, 8, and 9. For each ROI, the average hemodynamic response to each condition was computed and then normalized by the average hemodynamic offset to yield a percent signal change. These values were then averaged across subjects. Since two of the macaques were scanned at 1.5 T while two were scanned at 3 T, prior to averaging between 1.5 T and 3 T data, the activations in each macaque subject were normalized by the average response across all visual areas to a zero disparity random-dot pattern versus uniform gray (measured during the same scan session).

Acknowledgments

We are grateful to Egon Pasztor for building the barrel chair and to Doug Greve, Bruce Fischl, Rick Hoge, Don Rogers, Mike Lafratta, Koen Nelissen, and Katrien Denys for technical support. Greg DeAngelis, James Lewis, David Hubel, Bevil Conway, Winrich Freiwald, and Robert Savoy provided helpful discussions and comments on the manuscript. This work was supported by grants from the MIND Institute, NIH (1RO1MH67529), BRP (1RO1EB00790), the Queen Elisabeth Foundation (GSKE), NFWO (G3106.94 and G0112.00), GOA (95/6 and 2000/11), and IUAP (4/22).

Received: July 30, 2002
Revised: June 5, 2003
Accepted: July 3, 2003
Published: July 30, 2003

References

Adams, D.L., and Zeki, S. (2001). Functional organization of macaque V3 for stereoscopic depth. J. Neurophysiol. *86*, 2195–2203.

Allman, J.M. (1999). Evolving Brains (New York: W.H. Freeman).

Backus, B.T., Fleet, D.J., Parker, A.J., and Heeger, D.J. (2001). Human cortical activity correlates with stereoscopic depth perception. J. Neurophysiol. *86*, 2054–2068.

Barlow, H.B., Blakemore, C., and Pettigrew, J.D. (1967). The neural mechanism of binocular depth discrimination. J. Physiol. *193*, 327–342.

Bradley, D.C., and Andersen, R.A. (1998). Center-surround antagonism based on disparity in primate area MT. J. Neurosci. *18*, 7552–7565.

Bradley, D.C., Chang, G.C., and Andersen, R.A. (1998). Encoding of three-dimensional structure-from-motion by primate area MT neurons. Nature *392*, 714–717.

Corbetta, M., Akbudak, E., Conturo, T.E., Snyder, A.Z., Ollinger, J.M., Drury, H.A., Linenweber, M.R., Petersen, S.E., Raichle, M.E., Van Essen, D.C., and Shulman, G.L. (1998). A common network of functional areas for attention and eye movements. Neuron *21*, 761–773.

Cox, R.W., and Hyde, J.S. (1997). Software tools for analysis and visualization of FMRI data. NMR Biomed. *10*, 171–178.

Crone, R.A., and Leuridan, O.M.A. (1973). Tolerance for aniseikonia. I. Diplopia thresholds in the vertical and horizontal meridians of the visual field. Albrecht v Graefes Archiv fur Ophthalmologie *188*, 1–16.

Dale, A.M., Fischl, B., and Sereno, M.I. (1999). Cortical surface-based analysis. I. Segmentation and surface reconstruction. Neuroimage *9*, 179–194.

DeAngelis, G.C., and Newsome, W.T. (1999). Organization of disparity-selective neurons in macaque area MT. J. Neurosci. *19*, 1398–1415.

DeAngelis, G.C., and Uka, T. (2003). Coding of horizontal disparity and velocity by MT neurons in the alert macaque. J. Neurophysiol. *89*, 1094–1111.

DeAngelis, G.C., Cumming, B.G., and Newsome, W.T. (1998). Cortical area MT and the perception of stereoscopic depth. Nature *394*, 677–680.

DeYoe, E.A., Carman, G.J., Bandettini, P., Glickman, S., Wieser, J., Cox, R., Miller, D., and Neitz, J. (1996). Mapping striate and extrastriate visual areas in human cerebral cortex. Proc. Natl. Acad. Sci. USA *93*, 2382–2386.

Eifuku, S., and Wurtz, R.H. (1999). Response to motion in extrastriate area MSTl: disparity sensitivity. J. Neurophysiol. *82*, 2462–2475.

Engel, S.A., Glover, G.H., and Wandell, B.A. (1997). Retinotopic organization in human visual cortex and the spatial precision of functional MRI. Cereb. Cortex *7*, 181–192.

Ferraina, S., Pare, M., and Wurtz, R.H. (2000). Disparity sensitivity of frontal eye field neurons. J. Neurophysiol. *83*, 625–629.

Fischl, B., Sereno, M.I., and Dale, A.M. (1999). Cortical surface-based analysis. II: Inflation, flattening, and a surface-based coordinate system. Neuroimage *9*, 195–207.

Galletti, C., Battaglini, P.P., and Fattori, P. (1990). "Real-motion" cells in area V3A of macaque visual cortex. Exp. Brain Res. *82*, 67–76.

Gaska, J.P., Jacobson, L.D., and Pollen, D. (1988). Spatial and temporal frequency selectivity of neurons in visual cortical area V3A of the macaque monkey. Vision Res. *28*, 1179–1191.

Gandhi, S., Heeger, D., and Boynton, G.M. (1999). Spatial attention affects brain activity in human primary visual cortex. Proc. Natl. Acad. Sci. USA *96*, 3314–3319.

Gilaie Dotan, S., Ullman, S., Kushnir, T., and Malach, R. (2002). Shape-selective stereo processing in human object-related visual areas. Hum. Brain Mapp. *15*, 67–79.

Gnadt, J., and Mays, L. (1995). Neurons in monkey parietal area lip are tuned for eye-movement parameters in three-dimensional space. J. Neurophysiol. *73*, 280–297.

Gonzalez, F., and Perez, R. (1998). Neural mechanisms underlying stereoscopic vision. Prog. Neurobiol. *55*, 191–224.

Greenlee, M.W., and Rutschmann, R.M. (2000). fMRI responses to binocular disparity in random-dot patterns. Invest. Opthalmol. Vis. Sci. (suppl) *41*, 735.

Grill-Spector, K., Kourtzi, Z., and Kanwisher, N. (2001). The lateral occipital complex and its role in object recognition. Vision Res. *41*, 1409–1422.

Hadjikhani, N., Liu, A.K., Dale, A.M., Cavanagh, P., and Tootell, R.B. (1998). Retinotopy and color sensitivity in human visual cortical area V8. Nat. Neurosci. *1*, 235–241.

Hinkle, D., and Connor, C. (2000). Disparity tuning in macaque area V4. Neuroreport *12*, 365–369.

Hubel, D.H., and Livingstone, M.S. (1987). Segregation of form, color, and stereopsis in primate area *18*. J. Neurosci. *7*, 3378–3415.

Hubel, D.H., and Wiesel, T.N. (1970). Stereoscopic vision in macaque monkey. Cells sensitive to binocular depth in area 18 of the macaque monkey cortex. Nature *225*, 41–42.

Janssen, P., Vogels, R., and Orban, G.A. (2000). Selectivity for 3D shape that reveals distinct areas within macaque inferior temporal cortex. Science *288*, 2054–2056.

Julesz, B. (1971). Foundations of Cyclopean Perception (Chicago, IL: University of Chicago Press).

Kastner, S., DeWeerd, P., Desimone, R., and Ungerleider, L.G. (1998). Mechanisms of directed attention in ventral extrastriate cortex as revealed by functional MRI. Science *282*, 108–111.

Kourtzi, Z., and Kanwisher, N. (2001). Representation of perceived object shape by the human lateral occipital complex. Science *293*, 1506–1509.

Krubitzer, L.A. (2000). How does evolution build a complex brain? Novartis Found. Symp. *228*, 206–220.

Kwee, I.L., Fujii, Y., Matsuzawa, H., and Nakada, T. (1999). Perceptual processing of stereopsis in humans: high-field (3.0-tesla) functional MRI study. Neurology *53*, 1599–1601.

Le, T.H., Pardo, J.V., and Hu, Z. (1998). 4T-fMRI study of nonspatial shifting of selective attention: cerebellar and parietal contributions. J. Neurophysiol. *79*, 1535–1548.

Leite, F.P., Tsao, D., Vanduffel, W., Fize, D., Sasaki, Y., Wald, L.L., Dale, A.M., Kwong, K.K., Orban, G.A., Rosen, B.R., et al. (2002). Repeated fMRI using iron oxide contrast agent in awake, behaving macaques at 3 Tesla. Neuroimage *16*, 283–294.

Lewis, J.W., and Van Essen, D.C. (2000a). Corticocortical connections of visual, sensorimotor, and multimodal processing areas in the parietal lobe of the macaque monkey. J. Comp. Neurol. *428*, 112–137.

Lewis, J.W., and Van Essen, D.C. (2000b). Mapping of architectonic subdivisions in the macaque monkey, with emphasis on parieto-occipital cortex. J. Comp. Neurol. *428*, 79–111.

Masson, G.S., Busettini, C., and Miles, F.A. (1997). Vergence eye movements in response to binocular disparity without depth perception. Nature *389*, 283–286.

Maunsell, J.H., and Van Essen, D.C. (1983). Functional properties of neurons in middle temporal visual area of the macaque monkey. II. Binocular interactions and sensitivity to binocular disparity. J. Neurophysiol. *49*, 1148–1167.

Mendola, J.D., Dale, A.M., Fischl, B., Liu, A.K., and Tootell, R.B. (1999). The representation of illusory and real contours in human cortical visual areas revealed by functional magnetic resonance imaging. J. Neurosci. *19*, 8560–8572.

Mountcastle, V.B., Lynch, J.C., Georgopoulos, A., Sakata, H., and Acuna, C. (1975). Posterior parietal association cortex of the monkey: command functions for operations within extrapersonal space. J. Neurophysiol. *38*, 871–908.

Nakamura, H., Kuroda, T., Wakita, M., Kusunoki, M., Kato, A., Mikami, A., Sakata, H., and Itoh, K. (2001). From three-dimensional

space vision to prehensile hand movements: the lateral intraparietal area links the area V3A and the anterior intraparietal area in macaques. J. Neurosci. *21*, 8174–8187.

Orban, G.A., Sunaert, S., Todd, J.T., Van Hecke, P., and Marchal, G. (1999). Human cortical regions involved in extracting depth from motion. Neuron *24*, 929–940.

Pettigrew, J.D., Nikara, T., and Bishop, P.O. (1968). Binocular interaction on single units in cat striate cortex: simultaneous stimulation by single moving slits with receptive fields in correspondence. Exp. Brain Res. *6*, 391–410.

Peuskens, H., Todd, J.T., Norman, F., Van Hecke, P., and Orban, G.A. (2002). Neural correlates of judging 3D structure from motion. J. Vis. *2*, 301.

Poggio, G.F., and Fischer, B. (1977). Bincoular interaction and depth sensitivity in striate and prestriate cortex of behaving rhesus monkey. J. Neurophysiol. *40*, 1392–1405.

Poggio, G., Gonzalez, F., and Krause, F. (1988). Stereoscopic mechanisms in monkey visual cortex: binocular correlation and disparity selectivity. J. Neurosci. *8*, 4531–4550.

Press, W.A., Brewer, A.A., Dougherty, R.F., Wade, A.R., and Wandell, B.A. (2001). Visual areas and spatial summation in human visual cortex. Vision Res. *41*, 1321–1332.

Robinson, D. (1972). Eye movement evoked by collicular stimulation in the alert monkey. Vision Res. *12*, 1795–1808.

Roy, J.P., Komatsu, H., and Wurtz, R.H. (1992). Disparity sensitivity of neurons in monkey extrastriate area MST. J. Neurosci. *12*, 2478–2492.

Sakata, H., Taira, M., Kusunoki, M., Murata, A., Tanaka, Y., and Tsutsui, K. (1998). Neural coding of 3D features of objects for hand action in the parietal cortex of the monkey. Philos. Trans. R. Soc. Lond. B. Biol. Sci. *353*, 1363–1373.

Sasaki, Y., Hadjikhani, N., Fischl, B., Liu, A.K., Marret, S., Dale, A.M., and Tootell, R.B. (2001). Local and global attention are mapped retinotopically in human occipital cortex. Proc. Natl. Acad. Sci. USA *98*, 2077–2082.

Sereno, M.I., Dale, A.M., Reppas, J.B., Kwong, K.K., Belliveau, J.W., Brady, T.J., Rosen, B.R., and Tootell, R.B. (1995). Borders of multiple visual areas in humans revealed by functional magnetic resonance imaging. Science *268*, 889–893.

Shen, T., Weissleder, R., Papisov, M., Bogdanov, A., Jr., and Brady, T.J. (1993). Monocrystalline iron oxide nanocompounds (MION): physicochemical properties. Magn. Reson. Med. *29*, 599–604.

Snyder, L.H., Batista, A.P., and Andersen, R.A. (2000). Intention-related activity in the posterior parietal cortex: a review. Vision Res. *40*, 1433–1441.

Somers, D.C., Dale, A.M., Seiffert, A.E., and Tootell, R.B. (1999). Functional MRI reveals spatially specific attentional modulation in human primary visual cortex. Proc. Natl. Acad. Sci. USA *96*, 1663–1668.

Takemura, A., Inoue, Y., Kawano, K., Quaia, C., and Miles, F.A. (2001). Single unit activity in cortical area MST associated with disparity-vergence eye movements: evidence for population coding. J. Neurophysiol. *85*, 2245–2266.

Thier, P., and Karnath, H.-O. (1997). Parietal Lobe Contributions to Orientation in 3D Space, Volume 25 (Heidelberg: Springer-Verlag).

Thomas, O.M., Cumming, B.G., and Parker, A.J. (2002). A specialization for relative disparity in V2. Nat. Neurosci. *5*, 472–478.

Tootell, R.B., and Hadjikhani, N. (2001). Where is 'dorsal V4' in human visual cortex? Retinotopic, topographic and functional evidence. Cereb. Cortex *11*, 298–311.

Tootell, R.B., Reppas, J.B., Kwong, K.K., Malach, R., Born, R.T., Brady, T.J., Rosen, B.R., and Belliveau, J.W. (1995). Functional analysis of human MT and related visual cortical areas using magnetic resonance imaging. J. Neurosci. *15*, 3215–3230.

Tootell, R.B., Mendola, J.D., Hadjikhani, N.K., Ledden, P.J., Liu, A.K., Reppas, J.B., Sereno, M.I., and Dale, A.M. (1997). Functional analysis of V3A and related areas in human visual cortex. J. Neurosci. *17*, 7060–7078.

Tootell, R.B., Hadjikhani, N., Hall, E.K., Marrett, S., Vanduffel, W., Vaughan, J.T., and Dale, A.M. (1998a). The retinotopy of visual spatial attention. Neuron *21*, 1409–1422.

Tootell, R.B., Hadjikhani, N.K., Vanduffel, W., Liu, A.K., Mendola, J.D., Sereno, M.I., and Dale, A.M. (1998b). Functional analysis of primary visual cortex (V1) in humans. Proc. Natl. Acad. Sci. USA *95*, 811–817.

Ts'o, D.Y., Roe, A.W., and Gilbert, C.D. (2001). A hierarchy of the functional organization for color, form and disparity in primate visual area V2. Vision Res. *41*, 1333–1349.

Ungerleider, L., and Desimone, R. (1986). Cortical connections of visual area MT in the macaque. J. Comp. Neurol. *248*, 190–222.

Vanduffel, W., Fize, D., Mandeville, J.B., Nelissen, K., Van Hecke, P., Rosen, B.R., Tootell, R.B.H., and Orban, G.A. (2001). Visual motion processing investigated using contrast-agent enhanced fMRI in awake behaving monkeys. Neuron *32*, 565–577.

Vanduffel, W., Fize, D., Peuskens, H., Denys, K., Sunaert, S., Todd, J.T., and Orban, G.A. (2002). Extracting 3D from motion; differences in human and monkey intraparietal cortex. Science *298*, 413–415.

Van Essen, D.C. (2003). Organization of visual areas in macaque and human cerebral cortex. In The Visual Neurosciences, L. Chalupa and J. S. Werner, eds. (Cambridge, MA: MIT Press).

Van Essen, D.C., Dickson, J., Harwell, J., Hanlon, D., Anderson, C.H., and Drury, H.A. (2001). An integrated software system for surface-based analyses of cerebral cortex. J. Am. Med. Inform. Assoc. *8*, 443–459.

Watanabe, M., Tanaka, H., Uka, T., and Fujita, I. (2002). Disparity-selective neurons in area V4 of macaque monkeys. J. Neurophysiol. *87*, 1960–1973.

Wojciulik, E., and Kanwisher, N. (1999). The generality of parietal involvement in visual attention. Neuron *23*, 747–764.

Xiao, D.-K., Marcar, V.L., Raiguel, S.E., and Orban, G.A. (1997). Selectivity of macaque MT/V5 neurons for surface orienation in depth specified by motion. Eur. J. Neurosci. *9*, 956–964.

Zeki, S.M. (1978). The third visual complex of rhesus monkey prestriate cortex. J. Physiol. *277*, 245–272.